

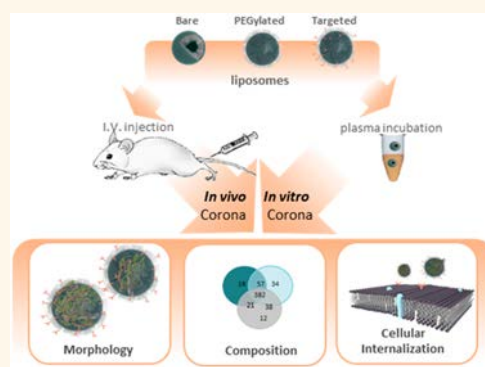
# *In Vivo* Biomolecule Corona around Blood-Circulating, Clinically Used and Antibody-Targeted Lipid Bilayer Nanoscale Vesicles

Marilena Hadjidemetriou,<sup>†</sup> Zahraa Al-Ahmady,<sup>†</sup> Mariarosa Mazza,<sup>†</sup> Richard F. Collins,<sup>‡</sup> Kenneth Dawson,<sup>§</sup> and Kostas Kostarelos<sup>\*,†</sup>

<sup>†</sup>Nanomedicine Lab, Institute of Inflammation and Repair; Faculty of Medical & Human Sciences; <sup>‡</sup>Electron Microscopy Facility, Faculty of Life Sciences, The University of Manchester, Manchester M13 9PT, United Kingdom and <sup>§</sup>Centre For BioNano Interactions (CBNI), School of Chemistry and Chemical Biology, University College Dublin, Belfield, Dublin 4, Ireland

**ABSTRACT** The adsorption of proteins and their layering onto nanoparticle surfaces has been called the “protein corona”. This dynamic process of protein adsorption has been extensively studied following *in vitro* incubation of many different nanoparticles with plasma proteins. However, the formation of protein corona under dynamic, *in vivo* conditions remains largely unexplored. Extrapolation of *in vitro* formed protein coronas to predict the fate and possible toxicological burden from nanoparticles *in vivo* is of great interest. However, complete lack of such direct comparisons for clinically used nanoparticles makes the study of *in vitro* and *in vivo* formed protein coronas of great importance. Our aim was to study the *in vivo* protein corona formed onto intravenously injected, clinically used liposomes, based on the composition of the PEGylated liposomal formulation that constitutes the anticancer agent Doxil. The formation of *in vivo* protein

corona was determined after the recovery of the liposomes from the blood circulation of CD-1 mice 10 min postinjection. In comparison, *in vitro* protein corona was formed by the incubation of liposomes in CD-1 mouse plasma. *In vivo* and *in vitro* formed protein coronas were compared in terms of morphology, composition and cellular internalization. The protein coronas on bare (non-PEGylated) and monoclonal antibody (IgG) targeted liposomes of the same lipid composition were also comparatively investigated. A network of linear fibrillary structures constituted the *in vitro* formed protein corona, whereas the *in vivo* corona had a different morphology but did not appear to coat the liposome surface entirely. Even though the total amount of protein attached on circulating liposomes correlated with that observed from *in vitro* incubations, the variety of molecular species in the *in vivo* corona were considerably wider. Both *in vitro* and *in vivo* formed protein coronas were found to significantly reduce receptor binding and cellular internalization of antibody-conjugated liposomes; however, the *in vivo* corona formation did not lead to complete ablation of their targeting capability.



**KEYWORDS:** protein corona · Doxil · fibrillation · nanomedicine · nanoparticle · nanotoxicology

Characterization of nanoparticles (NPs) in the biological milieu has been the focus of intense research over the past few years. It has been repeatedly reported that the synthetic identity of nanomaterials is instantly modified once they are dispersed in a biofluid, because of their tendency to interact with their surrounding biomolecules. Proteins physisorbed on NP surfaces form a complex bioshell, termed “protein corona”,<sup>1</sup> the composition of which is shaped by the physicochemical characteristics of NPs.<sup>2–4</sup> This dynamic process of

protein adsorption alters NP surface properties and is therefore considered to play a critical role in their overall biological behavior. Experiments performed *in vitro* demonstrated that the cytotoxicity,<sup>3,5,6</sup> cellular internalization<sup>7–11</sup> and targeting capability<sup>12–14</sup> of NPs significantly differ in the absence and presence of protein corona.

The interaction of proteins with nanomaterials has been a crucial factor for their design over the years. Early protein adsorption studies in the 80s and 90s aimed to develop adsorption-resistant nanomaterials

\* Address correspondence to [kostas.kostarelos@manchester.ac.uk](mailto:kostas.kostarelos@manchester.ac.uk).

Received for review April 14, 2015 and accepted July 2, 2015.

Published online July 02, 2015  
10.1021/acs.nano.5b03300

© 2015 American Chemical Society

to prevent opsonisation of NPs, and thus to increase their blood circulation time.<sup>15</sup> A major breakthrough was the surface coating of nanoparticles with the hydrophilic polymer polyethylene glycol (PEG), which imparts steric stabilization and reduces the interaction of NPs with serum proteins.<sup>16–18</sup> Although PEGylation is still the most widely used antiopsonisation strategy, it cannot fully prevent protein adsorption.<sup>19–21</sup> The PEG layer has also been found to interfere with the interaction of nanoparticles with cells<sup>19,22</sup> in a rather unpredictable manner depending on the molecular weight and branching of the PEG molecules.

Further surface functionalization of PEGylated NPs with targeting ligands was thought to alleviate the negative impact of PEG on the cellular internalization of NPs. According to this strategy, NPs will not only circulate longer in blood, but also recognize and bind to specific receptors expressed by target cells.<sup>23</sup> Despite the great amount of preclinical and clinical research work performed in the field of such actively targeted nanomedicines, their use in the clinical setting is yet to be established. In addition to physiological barriers that limit targeted NP accumulation into specific sites in the body, interaction of NPs with plasma proteins is considered to be one of the main reasons why ligand-targeted nanomedicines have failed so far in the clinic.<sup>12–14</sup>

Although the formation of protein coronas on the NP surface has been extensively investigated *in vitro*, the extrapolation of *in vitro* based studies to predict the identity and fate of NPs *in vivo* remains doubtful.<sup>20</sup> Incubation of NPs with low serum concentration or with only one protein species are considered oversimplified to simulate the complexity of the *in vivo* situation. To date, in the vast majority of protein corona studies NPs are characterized after their incubation with human plasma, with the ensuing assumption that the protein content and identity formed under such a static biological environment may reflect protein corona formation *in vivo*. However, important aspects like the dynamic nature of NPs in blood flow, interaction with moving cells, the molecularly vastly richer environment, or the impact of immune responses triggered after NP injection cannot be mimicked by *in vitro* incubation protocols in plasma.

Very few earlier studies have investigated the interaction of nanoscale particles with proteins after *in vivo* administration.<sup>24–27</sup> These studies used only one characterization technique, gel electrophoresis, which suffers from poor protein separation and low detection sensitivity.<sup>28</sup> More sophisticated characterization of the protein corona formed *in vivo* onto superparamagnetic nanoparticles was only recently reported by Sakulku *et al.*<sup>29</sup> This study suggested that the composition of protein corona formed onto the specific NPs used (PVA-coated iron oxide NPs, ~90 nm diameter) after *in vivo* (intravenous) administration can

significantly differ compared to *in vitro* incubation with rat serum.

The aim of the present study was to investigate the formation of protein coronas on clinically used liposomes following their intravenous administration in mice and determine the corona impact on the cellular internalization of the protein-coated liposomes recovered from blood circulation. A PEGylated liposome composition (HSPC:Chol:DSPE-PEG2000) that constitutes the basis of the anticancer agent Doxil was employed in this study because of its established clinical profile for the treatment of various neoplastic indications.<sup>30,31</sup> In order to investigate the influence of *in vivo* protein corona formation on actively targeted NPs, a monoclonal antibody-conjugated version of the above liposome system was prepared by use of a clinically trialed (full IgG) hCTMO-1, targeting the MUC-1 transmembrane glycoprotein. The up-regulation of MUC-1 antigen in the majority of epithelial cancers constitutes this an attractive target for cancer immunotherapy. In addition, bare (non-PEGylated) liposomes (HSPC:Chol) were also studied in comparison to determine the role of PEG in the suppression of the protein corona formation *in vitro* and *in vivo*. The protein coronas formed after intravenous administration of the three liposome nanoscale systems in CD-1 mice were characterized by recovering the liposomes from blood circulation 10 min postinjection. In parallel, *in vitro* protein corona, formed by incubation of liposomes with CD-1 mouse plasma, was also characterized. *In vivo* and *in vitro* formed protein coronas were compared in terms of structure, composition and impact on the cellular internalization of the recovered liposomes.

## RESULTS

**Physicochemical Characterization of Liposomes and Protein Corona-Coated Liposomes.** The chemical composition and some physicochemical characteristics of bare, PEGylated and monoclonal antibody-conjugated, targeted liposomes engineered for this study are summarized in Figure 1. The lipid composition and molar ratios among the individual components were chosen to match the exact liposome composition of the clinically used liposomal doxorubicin agent (Doxil). Targeted liposomes were prepared by the postinsertion of anti-MUC-1 antibody into preformed PEGylated liposomes, resulting in the presentation of the antibody at the outer surface of the lipid bilayer as previously described.<sup>15,32</sup> Antibody density on the surface of targeted liposomes was found to be 28.86  $\mu\text{g Ab}/\mu\text{mol lipid}$  at Ab:lipid 1:500 molar ratio, which corresponds to approximately 14 Ab molecules/liposome (Figure S1).

Dynamic light scattering (DLS),  $\zeta$ -potential measurements and negative stain transmission electron microscopy (TEM) were performed prior to plasma incubations to analyze the properties and morphology

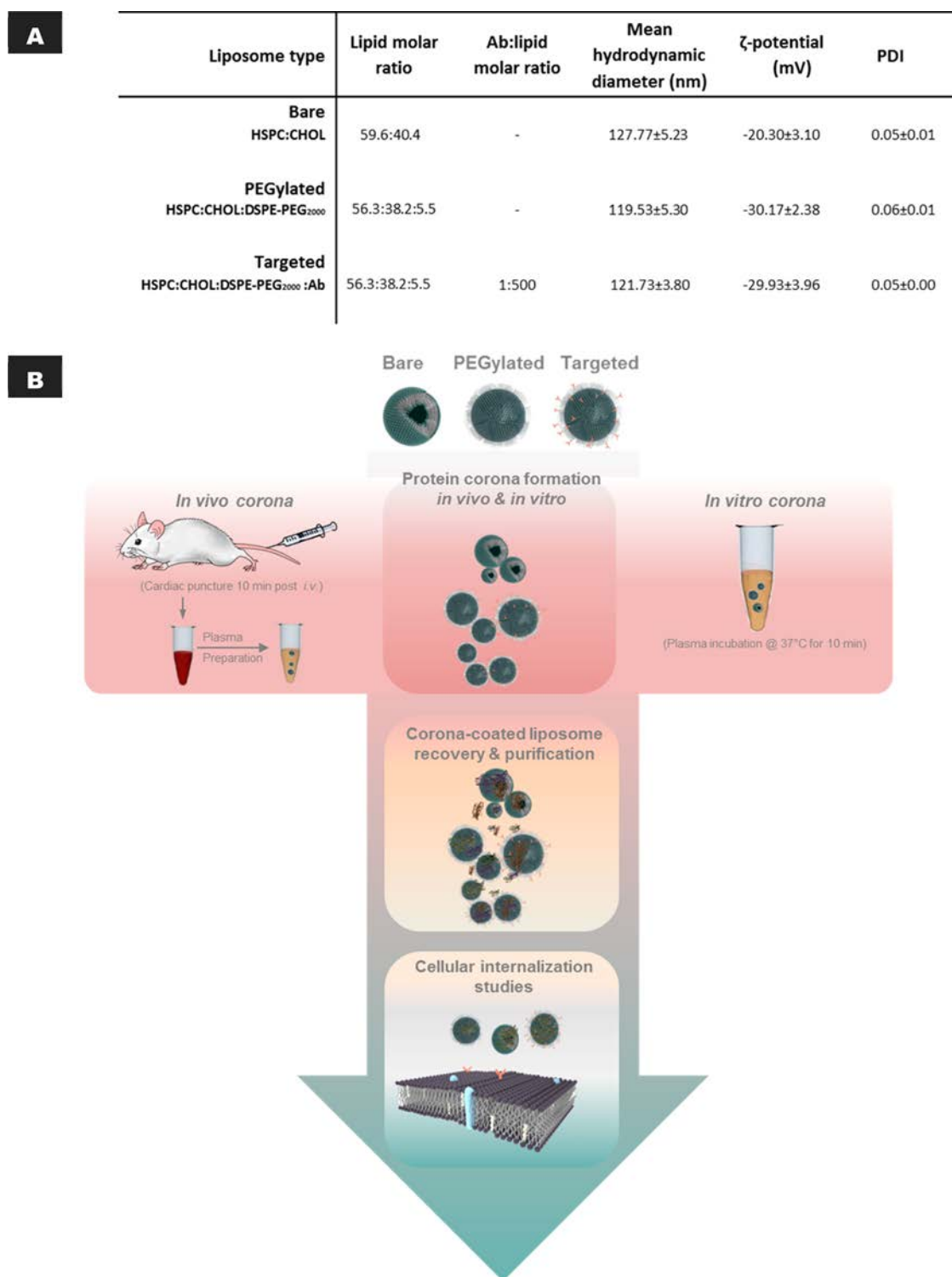
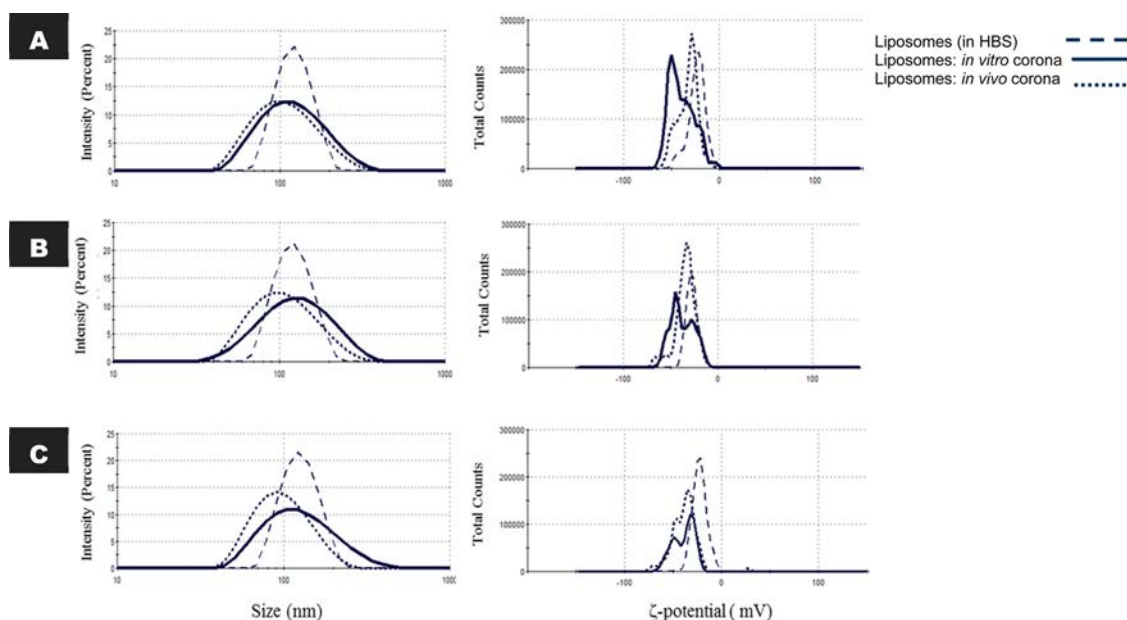


Figure 1. (A) Physicochemical characterization of liposomes. Mean hydrodynamic diameter (nm),  $\zeta$ -potential (mV) and polydispersity index (PDI) are shown. Values represent the average and standard error from three independent experiments. (HSPC, hydrogenated soy phosphatidylcholine; DSPE-PEG2000, 1,2-distearoyl-*sn*-glycero-3-phosphoethanolamine-N-[methoxy(polyethylene glycol)-2000; CHOL, cholesterol). (B) Schematic description of the experimental design including *in vivo* and *in vitro* protein corona formation. In the case of the *in vivo* corona formation, liposomes were administered intravenously (i.v.) via the tail vein ( $n = 3$  CD-1 mice/group; 3 independent experiments replicated) and 10 min postinjection were recovered by cardiac puncture. The plasma was then separated from the recovered blood by centrifugation. The *in vitro* corona was allowed to form on liposomes after incubation with isolated CD-1 mouse plasma for 10 min at 37 °C (3 independent experiments replicated). *In vivo* and *in vitro* protein-coated liposomes were purified from unbound proteins and used for cellular internalization studies.



**Figure 2.** The effect of protein corona formation on the physicochemical characteristics of liposomes. Mean diameter (nm) and  $\zeta$ -potential (mV) distributions are depicted for (A) bare; (B) PEGylated; and (C) targeted liposome systems, before and after their interaction with CD-1 mouse plasma *in vitro* and *in vivo*.

of bare liposomes. All three liposome systems had a mean hydrodynamic diameter between 110 and 130 nm and a negative surface charge of 20–30 mV. All liposomal formulations displayed low polydispersity values ( $<0.06$ ) indicating a narrow size distribution (Figure 1A; Figure 2). TEM imaging showed well-dispersed, round shaped vesicles, their size correlating that of DLS measurements (Figure 3A).

Protein corona has been described to form very rapidly following incubation of NPs with plasma proteins.<sup>33</sup> Because of this and the fact that bare (non-PEGylated) liposomes have a short blood circulation half-life, we chose to assess protein corona formation 10 min postincubation with plasma (*in vitro* corona) or postinjection (*in vivo* corona). To investigate the formation of a protein corona onto the vesicle surface *in vivo*, liposomes were first administered intravenously *via* tail vein injection into CD-1 mice and 10 min postinjection liposomes were recovered by cardiac puncture as shown in Figure 1B. Plasma was then prepared from recovered blood by centrifugation (see Experimental Section for further details). Protein corona was allowed to form onto vesicles *in vitro* as previously described by others,<sup>34–36</sup> by incubating the three liposome systems with CD-1 mouse plasma at 37 °C for 10 min under continuous agitation to mimic as much as possible the *in vivo* conditions. To confirm that the commercially available plasma used for our *in vitro* studies had the same composition as the plasma obtained from the *in vivo* experiments we performed mass spectrometry (Figure S2).

A protocol was developed in this study for the isolation of liposomes from unbound and loosely bound plasma proteins by combination of size

exclusion chromatography and membrane ultrafiltration. Although centrifugation has been the predominant methodology for the separation of protein-coated NPs following their exposure to biological fluids, for low-density NPs, such as liposomes, this method may not be applicable. In addition, strong centrifugation forces may modify the NP-protein interactions and promote protein aggregation. Size exclusion chromatography has been used previously for the separation of liposomes from proteins.<sup>37</sup> However, to ensure the separation of large proteins and protein aggregates, further membrane ultrafiltration was employed as a second purification step (Figure S3). The protocol developed here is thought to allow only the retention of the tightly adsorbed proteins onto the liposome surface, also referred to as the “hard corona”.

Liposomes were recovered and isolated from the blood circulation of CD-1 mice, as well as from *in vitro* incubation in CD-1 mouse plasma. The surface charge of liposomes shifted toward more negative values after their interaction with plasma proteins both *in vitro* and *in vivo* (Figure 2; Table S1). Dynamic light scattering measurements of protein corona-coated liposomes demonstrated that their size distribution broadened (larger polydispersity index). Formation of a protein corona can be usually manifested as an increase in the mean nanoparticle diameter since a layer of protein molecules is deposited onto their surface. In the case of liposomes, however, due to their elastic, softer structure the interaction with proteins is more complex, and it can lead to an increase in their mean diameter or to a reduction due to osmotically driven “shrinkage”, as previously reported by others<sup>38</sup> and also observed here (Table S1).

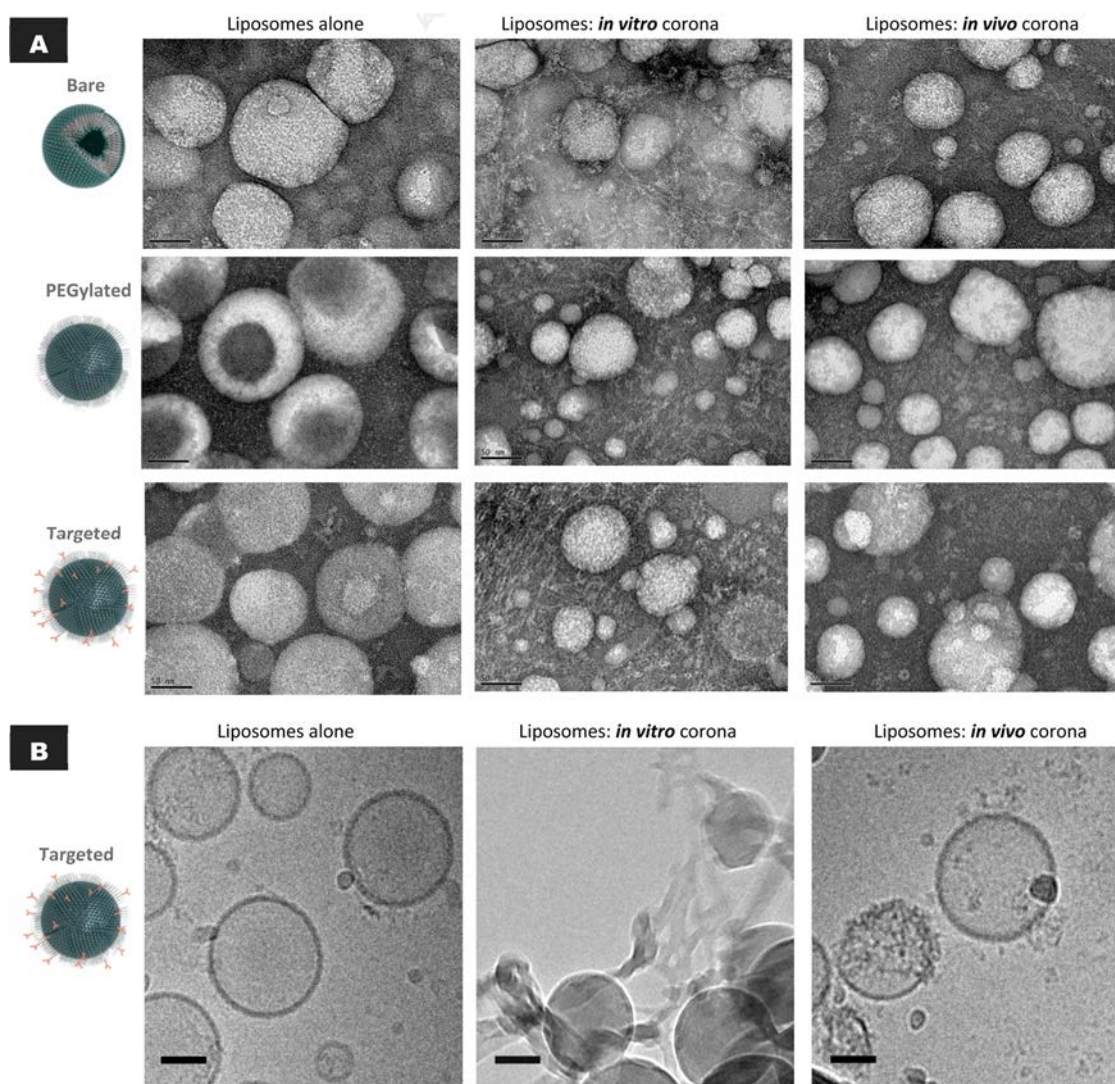


**Figure 3.** Morphological and structural characterization of liposomes before and after protein corona formation *in vitro* and *in vivo* by electron microscopy. (A) Negative stain TEM imaging showing the interaction of plasma proteins with bare, PEGylated and targeted liposomes, recovered from the blood circulation of CD-1 mice 10 min postinjection and from *in vitro* incubation with isolated CD-1 mouse plasma; and (B) Cryo-EM imaging of targeted liposomes before and after their *in vitro* and *in vivo* interaction with plasma proteins. All scale bars are 50 nm.

The overall colloidal characteristics of the liposomes recovered from the blood circulation of CD-1 mice were similar to those observed for liposomes isolated from *in vitro* plasma incubation. Also, the structural integrity of all liposome systems after recovery and isolation from blood (*in vivo*) or plasma (*in vitro*) as shown by TEM remained intact (Figure 3A).

**Characterization of Protein Corona.** TEM revealed that the structure of the protein corona formed onto liposomes in blood (*in vivo*) and in plasma (*in vitro*) was dramatically different morphologically. An expanded network of linear fibrillar structures formed only in the case of *in vitro* corona, while the *in vivo* corona appeared to have a more compact structure adsorbing onto the vesicle surface (Figure 3). Cryo-EM of the MoAb-conjugated (targeted) liposome system provided further evidence to confirm that the structure of the

corona forming around the liposomes after *in vitro* plasma incubation resulted in the assembly of fibrillar structures contrary to that observed *in vivo* (Figure 3B). The absence of fibrillar structures in CD-1 mouse plasma alone (without liposomes) (Figure S2) was a further indication that the assembly of the fibrillar structures observed was a result of the interaction with liposomes; however, more work would be needed to explore this further.

The next step was to quantitatively and qualitatively compare the *in vitro* and *in vivo* protein adsorption profiles for the three different types of liposomes. To compare the amount of proteins adsorbed, we calculated the protein binding ability (Pb), defined as the amount of protein associated with each  $\mu\text{mol}$  of lipid. As shown in Figure 4A, Pb values determined from *in vitro* incubation of each liposome type with

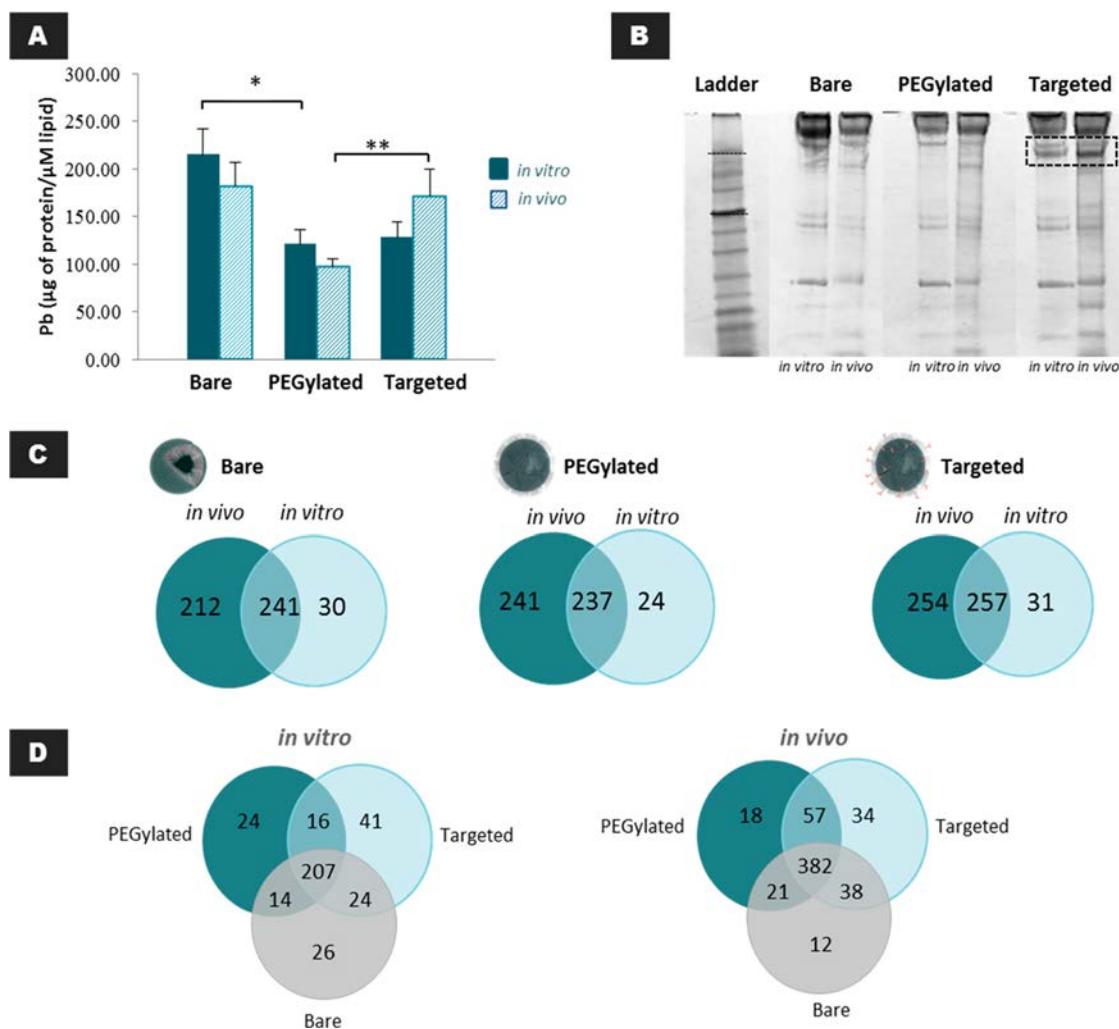


**Figure 4.** Comparison of protein adsorption profiles of bare, PEGylated and targeted liposomes after *in vivo* and *in vitro* protein corona formation. (A) Comparison of the amount of proteins adsorbed onto bare, PEGylated and targeted liposomes. In the case of targeted liposomes the amount of protein contributed by the conjugated Ab has been subtracted. Pb values ( $\mu\text{g}$  of protein/ $\mu\text{M}$  lipid) represent the average and standard error from three independent experiments, each using three mice per liposome system. \* indicates  $p < 0.05$  and \*\* indicates  $p < 0.01$ . (B) EZ-Blue stained SDS-PAGE gel of proteins associated with liposomes *in vitro* and *in vivo*. Selected area indicates the anti-MUC1 Ab. (C) Venn diagrams report the number of unique proteins identified in the *in vitro* and *in vivo* formed coronas and their respective overlap. (D) The effect of PEGylation and anti-MUC-1 Ab conjugation on the protein motifs observed *in vitro* and *in vivo*. Venn diagrams report the number of unique proteins identified in each of the three liposomal formulations and their respective overlap.

plasma were of the same range to those determined for liposomes isolated from the blood circulation of CD-1 mice. Therefore, the total amount of protein bound onto each liposome type was considered equivalent. However, comparison between bare and PEGylated liposomes indicated twice the amount of total protein adsorbed. Among PEGylated and targeted liposomes, total protein absorbed was almost of equal amounts *in vitro*; however, the presence of the full IgG antibody at the distal end of liposomes seemed to considerably increase the amount of blood proteins adsorbed *in vivo*. We attribute this phenomenon to the 34 unique proteins adsorbed only onto targeted liposomes *in vivo* as shown in Figure 4D that possibly interacted with anti-MUC-1 IgG antibody *via* protein–protein interactions.

Proteins associated with all liposome types *in vitro* and *in vivo* were separated by SDS-PAGE and visualized with Coomassie Brilliant Blue staining (Figure 4B). Qualitative differences were observed between the *in vitro* and *in vivo* protein coronas for all the three liposomal formulations. In agreement with protein quantification results, bare liposomes were found to adsorb the highest amount of proteins. Only minor differences were observed between protein coronas that formed onto PEGylated and targeted liposomes *in vitro*, whereas the corresponding *in vivo* adsorption profiles significantly differ. SDS-PAGE also confirmed that the targeting MoAb remained attached on the surface of targeted liposomes after the *in vitro* and *in vivo* protein corona formation and subsequent processing.

Bare		PEGylated		Targeted	
In vitro	In vivo	In vitro	In vivo	In vitro	In vivo
Identified Protein	RPA	Identified Protein	RPA	Identified Protein	RPA
Apolipoprotein E	5.55±1.54	Apolipoprotein C-III	4.93±1.64	Apolipoprotein E	5.74±0.83
Alpha-2-macroglobulin	5.33±1.57	Apolipoprotein E	3.54±0.59	Fibrinogen beta chain	4.86±0.45
<b>Fibrinogen beta chain</b>	<b>5.03±1.46</b>	Haemoglobin subunit beta-1	3.34±0.84	Alpha-2-macroglobulin	3.75±0.91
<b>Fibrinogen gamma chain</b>	<b>3.35±1.00</b>	Beta-globin	3.17±0.68	<b>Fibrinogen gamma chain</b>	<b>3.38±1.17</b>
Ig mu chain C region	3.18±0.50	Alpha-2-macroglobulin	2.96±0.64	Protein Fga	3.27±0.44
Protein Fga	3.00±0.95	Alpha globin 1	2.00±0.34	Ig kappa chain C region	2.67±0.38
Apolipoprotein C-III	2.09±0.47	Ig mu chain C region	1.99±0.16	Apolipoprotein B-100	2.37±0.42
Apolipoprotein C-I	2.00±0.94	Serum albumin	1.87±1.47	Apolipoprotein C-III	2.13±0.18
Apolipoprotein B-100	1.88±0.42	Hemoglobin subunit beta-2	1.84±1.20	Ig mu chain C region	2.04±0.43
Serum albumin	1.87±0.90	Apolipoprotein A-I	1.46±0.39	Serum albumin	1.75±0.45
Ig kappa chain C region	1.84±0.64	Apolipoprotein C-I	1.37±0.25	Haemoglobin subunit beta-1	1.69±0.29
Haemoglobin subunit beta-1	1.79±0.07	<b>Fibrinogen beta chain</b>	<b>1.35±0.86</b>	Haemoglobin subunit beta-2	1.54±0.31
Ig heavy chain V region	1.51±0.29	Apolipoprotein B-100	1.21±0.26	Thrombospondin-1	1.34±0.21
Thrombospondin-1	1.44±0.34	<b>Fibrinogen gamma chain</b>	<b>1.17±0.77</b>	Beta-globin	1.33±0.82
Ig heavy chain V-III region	1.35±0.45	Ig heavy chain V-III	1.12±0.51	Ig heavy chain V-III region	1.28±0.45
Apolipoprotein A-I	1.20±0.45	Mannose-binding protein C	1.07±0.11	Actin, cytoplasmic 1	1.22±0.18
Alpha globin 1	1.20±0.42	Apolipoprotein C-IV	0.99±0.33	Complement C3	1.21±0.15
Alpha-1B-glycoprotein	1.06±0.05	Apolipoprotein C-II	0.99±0.57	Complement C1q subcomponent subunit B	1.17±0.15
Serotransferrin	1.04±0.50	Complement C3	0.96±0.20	Ig heavy chain V region	1.16±0.28
Actin, cytoplasmic 1	1.04±0.23	Apolipoprotein A-II	0.90±0.19	Alpha globin 1	1.13±0.19
				Actin, cytoplasmic 1	0.76±0.04
				Complement C3	0.92±0.09
				Serum albumin	0.84±0.09
				Thrombospondin-1	1.32±0.10
				Apolipoprotein A-I	1.40±0.28
				Ig kappa chain C region	1.38±0.42
				Complement C3	1.38±0.42
				Vitronectin	0.84±0.20
				Thrombospondin-1	1.32±0.10
				Apolipoprotein A-I	1.40±0.28
				Ig kappa chain C region	1.38±0.42
				Complement C3	1.38±0.42
				Vitronectin	0.84±0.20
				Thrombospondin-1	1.32±0.10
				Apolipoprotein A-I	1.40±0.28
				Ig kappa chain C region	1.38±0.42
				Complement C3	1.38±0.42
				Vitronectin	0.84±0.20
				Thrombospondin-1	1.32±0.10
				Apolipoprotein A-I	1.40±0.28
				Ig kappa chain C region	1.38±0.42
				Complement C3	1.38±0.42
				Vitronectin	0.84±0.20
				Thrombospondin-1	1.32±0.10
				Apolipoprotein A-I	1.40±0.28
				Ig kappa chain C region	1.38±0.42
				Complement C3	1.38±0.42
				Vitronectin	0.84±0.20
				Thrombospondin-1	1.32±0.10
				Apolipoprotein A-I	1.40±0.28
				Ig kappa chain C region	1.38±0.42
				Complement C3	1.38±0.42
				Vitronectin	0.84±0.20
				Thrombospondin-1	1.32±0.10
				Apolipoprotein A-I	1.40±0.28
				Ig kappa chain C region	1.38±0.42
				Complement C3	1.38±0.42
				Vitronectin	0.84±0.20
				Thrombospondin-1	1.32±0.10
				Apolipoprotein A-I	1.40±0.28
				Ig kappa chain C region	1.38±0.42
				Complement C3	1.38±0.42
				Vitronectin	0.84±0.20
				Thrombospondin-1	1.32±0.10
				Apolipoprotein A-I	1.40±0.28
				Ig kappa chain C region	1.38±0.42
				Complement C3	1.38±0.42
				Vitronectin	0.84±0.20
				Thrombospondin-1	1.32±0.10
				Apolipoprotein A-I	1.40±0.28
				Ig kappa chain C region	1.38±0.42
				Complement C3	1.38±0.42
				Vitronectin	0.84±0.20
				Thrombospondin-1	1.32±0.10
				Apolipoprotein A-I	1.40±0.28
				Ig kappa chain C region	1.38±0.42
				Complement C3	1.38±0.42
				Vitronectin	0.84±0.20
				Thrombospondin-1	1.32±0.10
				Apolipoprotein A-I	1.40±0.28
				Ig kappa chain C region	1.38±0.42
				Complement C3	1.38±0.42
				Vitronectin	0.84±0.20
				Thrombospondin-1	1.32±0.10
				Apolipoprotein A-I	1.40±0.28
				Ig kappa chain C region	1.38±0.42
				Complement C3	1.38±0.42
				Vitronectin	0.84±0.20
				Thrombospondin-1	1.32±0.10
				Apolipoprotein A-I	1.40±0.28
				Ig kappa chain C region	1.38±0.42
				Complement C3	1.38±0.42
				Vitronectin	0.84±0.20
				Thrombospondin-1	1.32±0.10
				Apolipoprotein A-I	1.40±0.28
				Ig kappa chain C region	1.38±0.42
				Complement C3	1.38±0.42
				Vitronectin	0.84±0.20
				Thrombospondin-1	1.32±0.10
				Apolipoprotein A-I	1.40±0.28
				Ig kappa chain C region	1.38±0.42
				Complement C3	1.38±0.42
				Vitronectin	0.84±0.20
				Thrombospondin-1	1.32±0.10
				Apolipoprotein A-I	1.40±0.28
				Ig kappa chain C region	1.38±0.42
				Complement C3	1.38±0.42
				Vitronectin	0.84±0.20
				Thrombospondin-1	1.32±0.10
				Apolipoprotein A-I	1.40±0.28
				Ig kappa chain C region	1.38±0.42
				Complement C3	1.38±0.42
				Vitronectin	0.84±0.20
				Thrombospondin-1	1.32±0.10
				Apolipoprotein A-I	1.40±0.28
				Ig kappa chain C region	1.38±0.42
				Complement C3	1.38±0.42
				Vitronectin	0.84±0.20
				Thrombospondin-1	1.32±0.10
				Apolipoprotein A-I	1.40±0.28
				Ig kappa chain C region	1.38±0.42
				Complement C3	1.38±0.42
				Vitronectin	0.84±0.20
				Thrombospondin-1	1.32±0.10
				Apolipoprotein A-I	1.40±0.28
				Ig kappa chain C region	1.38±0.42
				Complement C3	1.38±0.42
				Vitronectin	0.84±0.20
				Thrombospondin-1	1.32±0.10
				Apolipoprotein A-I	1.40±0.28
				Ig kappa chain C region	1.38±0.42
				Complement C3	1.38±0.42
				Vitronectin	0.84±0.20
				Thrombospondin-1	1.32±0.10
				Apolipoprotein A-I	1.40±0.28
				Ig kappa chain C region	1.38±0.42
				Complement C3	1.38±0.42
				Vitronectin	0.84±0.20
				Thrombospondin-1	1.32±0.10
				Apolipoprotein A-I	1.40±0.28
				Ig kappa chain C region	1.38±0.42
				Complement C3	1.38±0.42
				Vitronectin	0.84±0.20
				Thrombospondin-1	1.32±0.10
				Apolipoprotein A-I	1.40±0.28
				Ig kappa chain C region	1.38±0.42
				Complement C3	1.38±0.42
				Vitronectin	0.84±0.20
				Thrombospondin-1	1.32±0.10
				Apolipoprotein A-I	1.40±0.28
				Ig kappa chain C region	1.38±0.42
				Complement C3	1.38±0.42
				Vitronectin	0.84±0.20
				Thrombospondin-1	1.32±0.10
				Apolipoprotein A-I	1.40±0.28
				Ig kappa chain C region	1.38±0.42
				Complement C3	1.38±0.42
				Vitronectin	0.84±0.20
				Thrombospondin-1	1.32±0.10
				Apolipoprotein A-I	1.40±0.28
				Ig kappa chain C region	1.38±0.42
				Complement C3	1.38±0.42
				Vitronectin	0.84±0.20
				Thrombospondin-1	1.32±0.10
				Apolipoprotein A-I	1.40±0.28
				Ig kappa chain C region	1.38±0.42
				Complement C3	1.38±0.42
				Vitronectin	0.84±0.20
				Thrombospondin-1	1.32±0.10
				Apolipoprotein A-I	1.40±0.28
				Ig kappa chain C region	1.38±0.42
				Complement C3	1.38±0.42
				Vitronectin	0.84±0.20
				Thrombospondin-1	1.32±0.10
				Apolipoprotein A-I	1.40±0.28
				Ig kappa chain C region	1.38±0.42
				Complement C3	1.38±0.42
				Vitronectin	0.84±0.20
				Thrombospondin-1	1.32±0.10
				Apolipoprotein A-I	1.40±0.28
				Ig kappa chain C region	1.38±0.42
				Complement C3	1.38±0.42
				Vitronectin	0.84±0.20
				Thrombospondin-1	1.32±0.10
				Apolipoprotein A-I	1.40±0.28
				Ig kappa chain C region	1.38±0.42
				Complement C3	1.38±0.42
				Vitronectin	0.84±0.20
				Thrombospondin-1	1.32±0.10
				Apolipoprotein A-I	1.40±0.28
				Ig kappa chain C region	1.38±0.42
				Complement C3	1.38±0.42
				Vitronectin	0.84±0.20
				Thrombospondin-1	1.32±0.10
				Apolipoprotein A-I	1.40±0.28
				Ig kappa chain C region	1.38±0.42
				Complement C3	1.38±0.42
				Vitronectin	0.84±0.20
				Thrombospondin-1	1.32±0.10
				Apolipoprotein A-I	1.40±0.28
				Ig kappa chain C region	1.38±0.42
				Complement C3	1.38±0.42
				Vitronectin	0.84±0.20
				Thrombospondin-1	1.32±0.10
				Apolipoprotein A-I	1.40±0.28
				Ig kappa chain C region	1.38±0.42
				Complement C3	1.38±0.42
				Vitronectin	0.84±0.20
				Thrombospondin-1	1.32±0.10
				Apolipoprotein A-I	1.40±0.28
				Ig kappa chain C region	1.38±0.42
				Complement C3	1.38±0.42
				Vitronectin	0.84±0.20
				Thrombospondin-1	1.32±0.10
				Apolipoprotein A-I	1.40±0.28
				Ig kappa chain C region</	

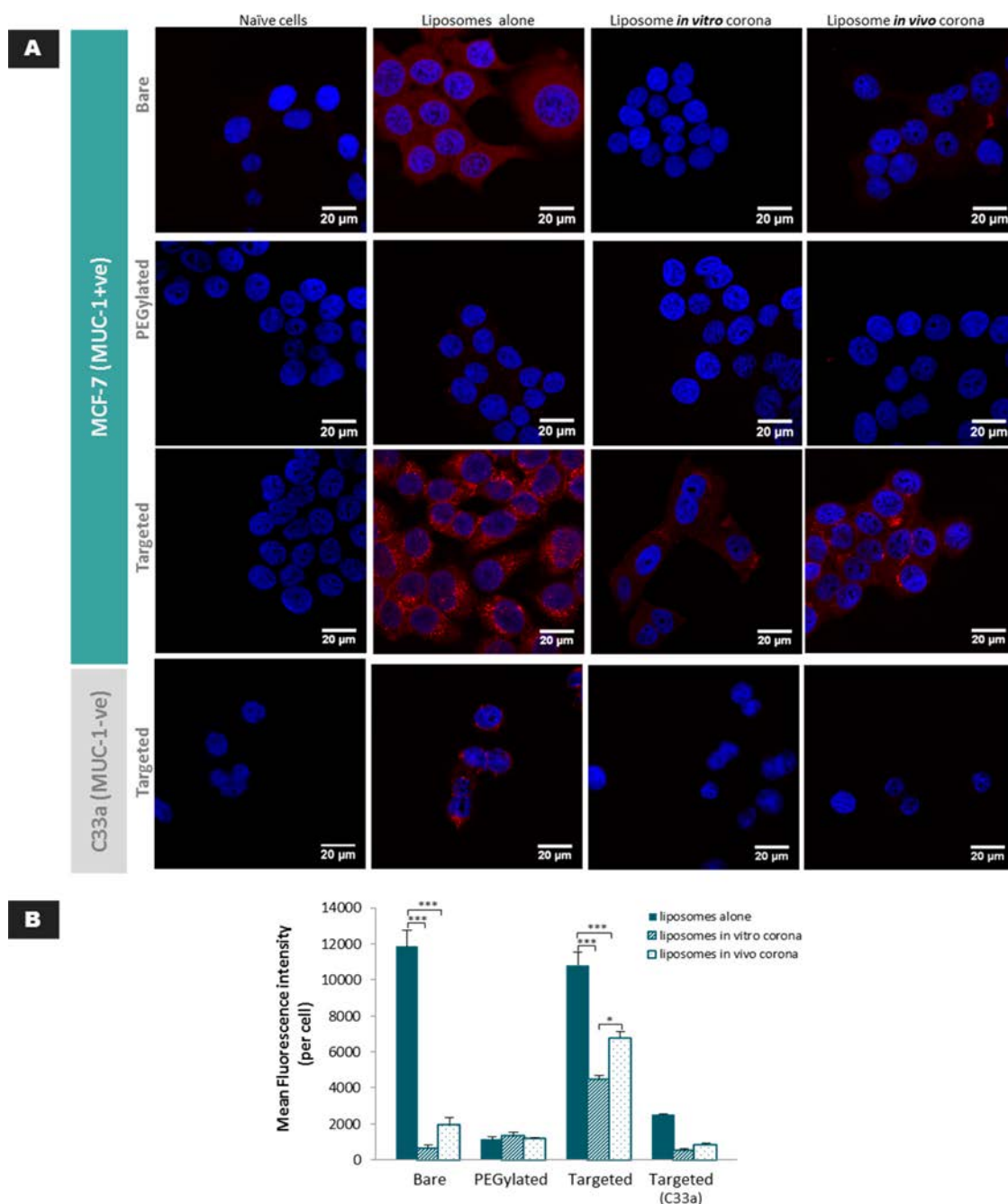


**Figure 6.** Cellular uptake studies of DiD labeled liposomes and protein-coated liposomes recovered from the circulation of CD-1 mice 10 min postinjection and from *in vitro* incubation with isolated plasma. (A) Confocal microscopy imaging of MCF7 cells shows the effect of protein corona on the internalization of DiD-labeled (red signal) bare and PEGylated liposomes 24 h after incubation. Confocal microscopy imaging of MCF7 cells (MUC-1+ve) and C33a cells (MUC-1-ve) shows the effect of protein corona on the targeting capability of DiD labeled (red signal) anti MUC-1 targeted liposomes. Nuclei were counterstained with DAPI (blue signal). (B) Fluorescence intensity measurements of the confocal microscopy images shown in A; \* indicates  $p < 0.05$  and \*\*\* indicates  $p < 0.005$ .

dye, DiD, in their phospholipid bilayer. Human epithelial cancer cells were incubated with liposomes before and after purification from *in vitro* incubation with mouse plasma and recovery from *in vivo* blood circulation (Figure 1). The use of MUC-1-positive (MCF-7) and MUC-1-negative (C33a) cell lines, allowed us to investigate the effect of protein coronas on receptor binding and internalization capability of the MoAb-targeted liposomes.

First, we examined the internalization of liposomes before their interaction with plasma proteins, 24 h post-incubation with MCF-7 cells. As illustrated in Figure 6, PEGylation inhibited the cellular uptake of liposomes. However, conjugation of the (anti-MUC-1) Ab significantly improved their cellular internalization, indicating binding specificity of the Ab to its antigen (MUC-1) and receptor-mediated endocytosis. To further confirm that

the internalization of targeted liposomes was due to the specific binding between Ab with the MUC-1 antigen, MUC-1-negative cells were incubated with targeted liposomes. 1 h postincubation, targeted liposomes were found to be internalized only by the MUC-1-positive cell line, whereas no detectable signal obtained in the case of MUC-negative cells (Figure S6). The weak signal observed 24 h postincubation of MUC-negative cells with targeted liposomes could be attributed to the internalization of liposomes by nonspecific interactions.

The effect of corona formation on the liposome cellular uptake was then studied. The isolation of liposomes from unbound and loosely bound proteins prior to cellular internalization experiments, allowed us to investigate how the *in vitro* and *in vivo* formed coronas impacted on liposome-cell interactions. Confocal microscopy demonstrated that although the overall uptake of bare liposomes within MCF-7 cells was diminished by both the *in vitro* and *in vivo* protein coronas, the effect was more pronounced in the case of *in vitro* corona-coated liposomes (Figure 6). PEGylated liposomes were very poorly internalized both before and after their interaction with plasma proteins, indicating that protein corona formation on the surface of PEGylated liposomes did not activate alternative pathways of internalization.

The importance of protein corona formation in determining liposome-cell interactions prompted us to evaluate its effect on actively (antibody) targeted liposomes. As depicted in Figure 6, both *in vitro* and *in vivo* protein coronas inhibited the interaction between the anti-MUC-1 antibody and the MUC-1 receptor, leading to reduced liposome internalization. However, the *in vitro* protein corona seemed to have a more significant inhibitory effect. MoAb-targeted liposomes recovered from blood circulation, seemed to be able to bind and internalize into MUC-1 positive cells despite the presence of the *in vivo* protein corona on their surface. We attributed that to the incomplete surface coating of the liposomes by the *in vivo* corona (as observed in Figure 3B) that allowed some antibodies to bind to MUC-1 receptors and initiate endocytosis into antigen-positive cells. Cell internalization experiments as early as 1 h after the incubation of cells with liposomes in the absence of serum in the cell culture media, before and after their *in vitro* and *in vivo* interaction with plasma proteins, further demonstrated the negative impact of the formed protein coronas on their binding and internalization efficiency (Figure S6).

## DISCUSSION

Any nanoparticle (NP) surface can be instantly modified once injected in the bloodstream by the formation of a protein corona.<sup>1</sup> According to this paradigm, the importance of the protein corona has been postulated as a determinant factor for the pharmacological and toxicological profile of NPs and will

impact significantly on their therapeutic capacity. Despite tremendous interest and a multitude of high-quality work that has reported the formation and characteristics (including the molecular composition) of the protein corona around NPs of different parametrization,<sup>11,42–45</sup> there is no report in the literature to describe the protein corona formed *in vivo* while in blood circulation onto NPs that are clinically used.

Early antiopsonisation studies highlighted that the amount of protein adsorbed onto liposomes can be used as an indicator of liposome longevity in blood circulation. Although these studies attempted to determine the amount of protein adsorbed onto different types of liposomes after their recovery from *in vivo* blood circulation, they did not investigate the molecular composition of protein corona.<sup>24–27</sup> Here, we attempted to offer a comprehensive comparison between the protein coronas that formed *in vitro* and *in vivo* on clinically established, PEGylated liposome systems of nanoscale dimensions. Bare (non-PEGylated) and antibody-targeted versions of the same liposome composition were investigated, to determine the ability of surface PEGylation to suppress protein adsorption, corona formation, as well as the effect of the protein corona on the targeting (binding and internalization) capability of liposomes within mammalian cell cultures.

Electron microscopy allowed assessment of liposome morphology after their interaction with plasma proteins *in vitro* and *in vivo* for 10 min, to indicate that in both cases liposomes remained structurally intact. Interestingly, all three liposome types incubated with mouse plasma *in vitro* resulted in the formation of fibrillar structures that interacted with the vesicles leading to extended clustering (Figure 3). These results provide previously unreported direct evidence of nanoparticle-mediated fibrillation in a complex biological fluid *in vitro* and should be investigated further more thoroughly. In contrast, no fibrillar structures were observed onto liposomes isolated following their *in vivo* blood circulation. This could be explained by the difference in protein composition between the *in vitro* and *in vivo* formed protein coronas (Figures 5 and S4).

In the case of promotion of a fibrillation process, the predominant hypothesis currently is that NPs can potentially act as platforms for protein adsorption and can enhance the probability of unfolded proteins to self-assemble.<sup>46</sup> The effect of different NPs on the fibrillation process has been mainly investigated in solutions of model-amyloidogenic proteins, under controlled conditions that promote protein aggregation.<sup>46–49</sup> Whether fibrillation can occur in a more complex biological fluid, where non-amyloidogenic proteins will compete for surface interactions onto the NP surface remains unexplored. Our data here strongly suggests that distinct differences exist between the *in vitro* and *in vivo* protein coronas that render the need for much more work beyond the scope of this study to draw

correlations between nanoparticle characteristics and the complexities of the interacting plasma environment (*in vitro* or *in vivo*; mouse or human) that may initiate or promote a process of fibrillation.

This work can also contribute to the discussion whether the incubation of NPs with plasma proteins *in vitro* can be considered as an accurate prediction of protein adsorption *in vivo*. Proteins bound onto intravenously injected liposomes and onto liposomes incubated with isolated plasma were quantitatively and qualitatively characterized. Although the total amount of liposome-associated proteins did not significantly vary *in vitro* and *in vivo*, protein corona *in vivo* was much more complex in terms of composition (Figure 4). The importance of characterizing plasma protein adsorption *in vivo* in order to more accurately predict the fate of liposomes was first emphasized by Chonn *et al.* in the early 90s.<sup>25</sup> In their study, gel electrophoresis was employed to demonstrate that while the amount of proteins attached on circulating liposomes correlated with that observed from *in vitro* plasma incubation, the type of proteins adsorbed considerably varied. A more precise comparison between the *in vitro* and *in vivo* formed protein coronas was very recently reported for non-clinically used, PVA-coated superparamagnetic NPs after their intravenous administration in rats.<sup>29</sup> In agreement with our results, mass spectrometry-based proteomic analysis in that study showed that the protein corona composition significantly differed between the *in vitro* and *in vivo* conditions; however, no information about the structural characteristics of the forming corona were offered.

On a broader context, our findings suggest that even though *in vitro* incubations of NPs with plasma proteins improve our understanding of the principles and mechanism of protein corona formation and self-assembly, their extrapolation to predict the pharmacological fate of NPs or their toxicological impact should be made with extreme caution. On the other hand, study of the *in vivo* protein coronas, although more reflective of the true biological environment with all its complexities, it is more challenging and limited by the low levels of recovered NPs. Moreover, it is also important to comprehend the potential limitations of extrapolating data from mice to humans. Caracciolo *et al.* have recently demonstrated that the *in vitro* incubation of PEGylated and non-PEGylated liposomes with mouse and human plasma results in different protein coronas suggesting that this could be a possible reason why some liposomal formulations work well in mice but fail to provide similar efficacy in humans.<sup>50</sup>

Identification of the corona proteins enabled us to correlate the liposome type with the protein molecules adsorbed both *in vitro* and *in vivo*. The majority of protein molecules were identical in terms of composition, but differed in total amount depending on the

liposome type. Pozzi *et al.* have previously reported significant overlap in the nature of protein molecules adsorbed onto cationic liposomes with and without PEG coating.<sup>19</sup> In agreement with our data PEGylation reduced the total amount of protein adsorbed onto the liposomes (Figure 4), but had a minor effect on the molecular consistency of the protein coronas. Interestingly, the targeted liposome systems that contained a full IgG MoAb at the distal end of some PEG chains led to corona formation of higher total protein content. The association of more proteins onto the surface of NPs in the presence of large molecular weight biological targeting ligands may also be relevant to other clinically used targeted, PEGylated constructs (*e.g.* PEGylated monoclonal antibody therapeutics such as Cimzia).

The different structural configuration and composition among the *in vitro* and *in vivo* formed protein coronas in our study, prompted us to assess their effect on the internalization of the liposomes within human epithelial cancer cells. It is now well-established that interactions of NPs with cells will be affected by the tightly bound corona proteins.<sup>51</sup> According to previous findings, the protein corona can either facilitate<sup>10,11,52</sup> or inhibit<sup>23</sup> the internalization of NPs. Confocal microscopy experiments in this study (Figure 6) demonstrated that both *in vitro* and *in vivo* protein coronas had an overall inhibiting role in the interactions of all liposomes with cells and their subsequent cell uptake. In addition, and in agreement with the literature, our data showed that modification of liposomes with a PEG surface layer reduced protein binding on the surface of liposomes,<sup>19</sup> but simultaneously inhibited the interaction of liposomes with cells.<sup>22</sup> Pozzi *et al.* recently suggested that the protein corona formed around PEGylated liposomes could determine receptor-binding and initiate endocytosis-mediated cell internalization, therefore could be exploited as an alternative strategy to achieve targeted delivery.<sup>53</sup> Such strategy could only be effective if target cells overexpressed the receptors specific to the corona-forming proteins, as has been discussed by others.<sup>54</sup> For example, cationic liposome/DNA complexes have been shown to specifically interact with vitronectin upon their incubation with human plasma, which enhances their uptake by cancer cells expressing vitronectin  $\alpha_v\beta_3$  receptor.<sup>52</sup> Nevertheless, in our study the inhibiting impact of PEGylation on the cellular internalization of liposomes was not alleviated following either *in vitro* or *in vivo* corona formation, even though this can be cell type specific.

Engineering of targeted liposomes with antibodies at the distal end of some of the PEG chains coating the vesicle surface was used as a strategy to interrogate the role of protein corona formation on receptor binding and cellular internalization. Conjugation of the full IgG anti-MUC-1 antibody dramatically improved their cellular internalization in serum-free conditions, while

plasma protein adsorption (*in vitro* or *in vivo*) and the formation of the protein corona were shown to significantly inhibit binding and uptake. However, in the case of *in vivo* protein corona formation, targeted liposome binding and internalization was more preserved and not entirely abolished (Figure 6). The impact of protein corona formed *in vitro* on the targeting capability of NPs has been investigated previously for silica,<sup>12,55</sup> gold<sup>14</sup> and polymeric NPs.<sup>56</sup> According to Salvati *et al.* the binding specificity of surface-bound transferrin for its receptor was lost in the presence of plasma proteins.<sup>12</sup> In that study, silica NPs (50 nm) grafted with PEG of various lengths with bound transferrin at their distal ends were incubated with lung epithelial cells in the presence and absence of serum proteins. Indeed, protein corona formed and blocked the transferrin-dependent internalization of NPs. The attachment of additional PEG chains on transferrin-targeted NPs did not improve their overall internalization efficiency. More recently, Dai *et al.*<sup>14</sup> further investigated the effect of PEG coating density and backfilling the surface of Herceptin-targeted, gold NPs (50 nm). This study concluded on some further design principles in order to allow restoration of binding specificity (lost due to protein corona formation) by coating with shorter PEG chains the NP surface, while allowing the targeting moiety to dangle from the distal end of longer PEG chains. In contrast, the targetability of EGR targeted silica NPs (97 nm) and huA33 mAb-functionalized polymeric nanoparticles (PMA) (2  $\mu$ m) has been shown to be retained in the presence of protein corona.<sup>55,56</sup> The contradictory results of these studies are not surprising, considering the unique character and morphology of the protein corona for each nanomaterial and the different binding affinities of the ligand-nanoparticle conjugates to their particular target receptors.<sup>56</sup>

Notably, no report today has studied the effect of protein corona formation on the targeting capability of clinically developed targeted NPs or targeted liposomes. Many types of actively targeted liposomes have reached clinical trials, but have failed clinically despite their outstanding *in vitro* and *in vivo* preclinical performance. One of the reasons for this discrepancy could be attributed to the findings of this study and others, suggesting significant loss of targetability and cellular uptake due to protein corona formation. However, the presence of a protein corona alone is not thought to be the sole reason for the therapeutic shortcomings of antibody-targeted liposomes, since efficacious tumor eradication has been repeatedly reported using different types of targeting ligands for different *in vivo* preclinical (commonly rodent) models.<sup>57–60</sup> The role of the protein corona on clinically developed liposomes should therefore be considered one of the contributing factors that will determine their pharmacological and biological performance, but not the sole critical factor.

## CONCLUSION

This study has revealed that the molecular complexity of the *in vivo* protein corona forming on clinically developed liposomes cannot be adequately predicted by their *in vitro* plasma incubations. Such complexity can lead to sharply different structural characteristics of the *in vivo* corona compared to that forming *in vitro*. Despite the substantial differences observed in the composition and morphology between *in vitro* and *in vivo* formed protein coronas, both restricted cellular internalization and compromised the targeting capability of MoAb-conjugated liposomes. We anticipate that this work will provide impetus for many more studies needed to reveal the characteristics of the forming *in vivo* protein coronas on different NP types and surface characteristics and their impact on the overall biological profile of these nanoparticles.

## EXPERIMENTAL SECTION

**Materials.** hCTMO1; anti MUC-1 IgG antibody (Ab) (150 kDa) was a kind gift from UCB (UK). Hydrogenated soy phosphatidylcholine (HSPC), 1,2-distearoyl-*sn*-glycero-3-phosphoethanolamine-*N*-[methoxy(polyethylene glycol)-2000] (DSPE-PEG2000) and 1,2-distearoyl-*sn*-glycero-3-phosphoethanolamine-*N*-[maleimide(polyethylene glycol)-2000] (ammonium salt) (Mal-DSPE-PEG2000) were purchased from Avanti Polar Lipids (USA), while cholesterol and 4-(2-Hydroxyethyl) piperazine-1-ethanesulfonic acid (HEPES) were purchased from Sigma (UK).

**Preparation of Liposomes.** Liposomes were prepared by thin lipid film hydration method followed by extrusion. Figure 1A shows the liposomal formulations employed, their lipid composition and the molar ratios. Briefly, lipids of different types were dissolved in chloroform:methanol mixture (4:1) in a total volume of 2 mL, using a 25 mL round-bottom flask. Organic solvents were then evaporated using a rotary evaporator (Buchi, Switzerland) at 40 °C, at 150 rotations/min, 1 h under a vacuum. Lipid films were hydrated with ammonium sulfate 250 mM (pH 8.5) at 60 °C to produce large multilamellar liposomes. Small unilamellar liposomes were then produced by extrusion through

800 and 200 nm polycarbonate filters (Whatman, VWR, UK) 10 times each and then 15 times through 100 and 80 nm extrusion filters (Whatman, VWR, UK) using a mini-Extruder (Avanti Polar Lipids, Alabaster, AL).

For the preparation of Targeted liposomes, PEGylated liposomes were first prepared as mentioned earlier followed by postinsertion of anti-MUC-1 mal-DSPE-PEG2000 micelles using the previously described<sup>15</sup> procedure. Mal-DSPE-PEG2000 micelles were prepared as followed: mal-DSPE-PEG2000 lipid was dissolved in chloroform:methanol mixture (4:1) in a total volume of 1 mL in a 25 mL round-bottom flask. Organic solvents were then evaporated with a rotary evaporator (Buchi, Switzerland), at 40 °C, at 150 rotations/min, under 1 h vacuum. mal-DSPE-PEG2000 lipid film was hydrated with HBS (20 mM HEPES, 150 mM NaCl, pH 7.4), at 60 °C. Anti-MUC-1 antibody was first thiolated as describe in Figure S1A by mixing with Traut's reagent (2-iminothiolane, Sigma, UK) at Ab:Traut's reagent molar ratio of 1:20 for 1 h at room temperature with continuous stirring at concentration of 10 mg Ab/mL buffer (25 mM HEPES, 140 mM NaCl, 3 mM EDTA, pH 8). Unreacted Traut's reagent was removed using Sephadex G50 column equilibrated with deoxygenated HBS (pH 7.4). The coupling reaction was run by mixing

thiolated Ab with mal-DSPE-PEG2000 micelles at 1:10 molar ratio in HBS (pH 7.4) overnight at room temperature. All Ab conjugation reactions were performed at oxygen free conditions. At the end of the reaction any uncoupled mal-DSPE-PEG2000 groups were blocked by mixing with cysteine HCl to a final concentration of 1 mM for 30 min. Ab micelles were then concentrated to 1 mL by centrifugation using Viva spin 6 columns (Sartorius, fisher) at 9000 rpm for 10–12 min. Mal-DSPE-PEG2000 Ab micelles were then post inserted into preformed PEGylated liposomes at Ab:lipids molar ratios 1:500, by 1 h incubation at 60 °C. Targeted liposomes were then separated from nonincorporated mal-DSPE-PEG2000 Ab micelles by using Sepharose CL-4B column in HBS (pH 7.4). Postinsertion efficiency was determined by collecting elution fractions (1 mL each) and analyzed spectrophotometrically for the presence of Ab (BCA protein assay) and liposomes (Stewart's assay) (Figure S1B).

For the BCA assay, a 6-point standard curve was generated by serial dilutions of BSA in HBS, with the top standard at a concentration of 2  $\mu\text{g}/\text{mL}$ . BCA reagent A and B were mixed at a ratio of 50:1 and 200  $\mu\text{L}$  of the BCA mixture were dispensed into a 96-well plate, in duplicates. Then, 25  $\mu\text{L}$  of each standard or unknown sample were added per well. The plate was incubated for 30 min at 37 °C, after which the absorbance was read at 574 nm on a plate reader (Fluostar Omega). Protein concentrations were calculated according to the standard curve. To quantify lipid concentration, 20  $\mu\text{L}$  of each samples was mixed with 1 mL of chloroform and 500  $\mu\text{L}$  of Stewart assay reagent in an Eppendorf tube. The samples were vortexed for 20 s followed by 1 min of centrifugation at 13 000 rpm. 200  $\mu\text{L}$  of the chloroform phase was transferred to a quartz cuvette. The optical density was measured on a using Cary 50 Bio Spectrophotometer (Agilent Technologies) at 485 nm. Lipid concentration was calculated according to a standard curve.

The conjugation of the anti-MUC-1 antibody to mal-DSPE-PEG2000 micelles was also confirmed by SDS-PAGE electrophoresis (Figure S1C). Briefly, 10  $\mu\text{L}$  of targeted liposomes were mixed with 10  $\mu\text{L}$  of Protein Solving Buffer (Fisher Scientific) and then boiled for 5 min at 90 °C. Twenty  $\mu\text{L}$  of each sample were then loaded in 10% Precise Tris-HEPES Protein Gel (Thermo Scientific). The gel was run for 1 h at 100 V in 50 times diluted Tris-HEPES SDS Buffer (Thermo Scientific). Staining was performed with EZ Blue Gel Staining reagent (Sigma Life Science) overnight followed by washing in distilled water for 2 h.

**Preparation of DiD-Labeled Liposomes.** To prepare DiD-labeled liposomes for cellular uptake studies, 5 mol % of DiD (Life Technologies) in ethanol (1 mg/mL) was added to the lipid mixture and liposomes were prepared by thin lipid film hydration method as described earlier. Lipid films were kept protected from light and purified by passing them through Sepharose CL-4B column (SIGMA-Aldrich) equilibrated with HBS (pH 7.4).

**Animal Experiments.** Eight to ten week old female CD1 mice were purchased from Charles River (UK). Animal procedures were performed in compliance with the UK Home Office Code of Practice for the Housing and Care of Animals used in Scientific Procedures. Mice were housed in groups of five with free access to water and kept at temperature of 19–22 °C and relative humidity of 45–65%. Before performing the procedures, animals were acclimatized to the environment for at least 7 days.

**Protein Corona Formation after *in Vivo* Administration.** CD1 mice were anesthetized by inhalation of isoflurane and liposomes were administered intravenously *via* the lateral tail vein, at a lipid dose of 0.125 mM/g body weight. This specific concentration was chosen because it is the equivalent lipid concentration to that of doxorubicin-loaded liposomes administered in pre-clinical studies to achieve a final doxorubicin dose of 5 mg/kg body weight.<sup>61–63</sup> Ten minutes after injection, liposomes were recovered from the blood by collection of ~0.5 mL blood samples, by cardiac puncture using K<sub>2</sub>EDTA coated blood collection tubes. Plasma was prepared by inverting 10 times the collection tubes to ensure mixing of blood with EDTA and subsequent centrifugation for 12 min at 1300 RCF at 4 °C. Supernatant was collected into Protein LoBind Eppendorf Tubes. The plasma samples obtained from three mice were pooled together.

**Protein Corona Formation after *in Vitro* Incubation with CD-1 Mice Plasma.** The *in vitro* formed corona was allowed to form using the same liposome concentration (2.25 mM) as that extracted in 1 mL of plasma from intravenously injected animals. For all *in vitro* protein binding studies, 2.25 mM of liposomes (180  $\mu\text{L}$  of 12.5 mM) were incubated with 820  $\mu\text{L}$  of CD-1 female mouse plasma (Seralab, UK, Batch # UU3110812) for 10 min at 37 °C in orbital shaker at 250 rpm setting to mimic *in vivo* conditions.

**Separation of Corona-Coated Liposomes from Unbound and Weakly Bound Proteins.** Liposomes recovered from *in vitro* and *in vivo* experiments were separated from excess plasma proteins by size exclusion chromatography followed by membrane ultrafiltration. Immediately after *in vitro* and *in vivo* incubations, 1 mL of plasma samples was loaded onto a Sepharose CL-4B (SIGMA-Aldrich) column (15 × 1.5 cm) equilibrated with HBS. Stewart assay in each chromatographic fraction (1 mL) revealed that liposomes were eluted in fractions 4,5 and 6 (Figure S3). Fractions containing liposomes were then pooled together and concentrated to 500  $\mu\text{L}$  by centrifugation using Vivaspin 6 column (10 000 MWCO, Sartorius, Fisher Scientific) at 9000 rpm Vivaspin 500 centrifugal concentrator (1 000 000 MWCO, Sartorius, Fisher Scientific) was then used at 9000 rpm, to further concentrate the samples to 100  $\mu\text{L}$  and to ensure separation of protein-coated liposomes from the remaining large unbound proteins. Liposomes were then washed 3 times with 100  $\mu\text{L}$  HBS to remove weakly bound proteins. To validate the separation of protein-coated liposomes from unbound proteins, the same procedure was performed with a control of plasma without liposomes (Figure S3).

**Size and Zeta Potential Measurements Using Dynamic Light Scattering (DLS).** Liposome size and surface charge were measured using Zetasizer Nano ZS (Malvern, Instruments, UK). For size measurement, samples were diluted with distilled water in 1 mL cuvettes. Zeta potential was measured in disposable Zetasizer cuvettes and sample dilution was performed with distilled water. Size and zeta potential data were taken in three and five measurements, respectively

**Transmission Electron Microscopy (TEM).** Liposomes of different compositions were visualized with transmission electron microscopy (FEI Tecnai 12 BioTwin) before and after their *in vitro* and *in vivo* interaction with plasma proteins. Samples were diluted to 1 mM lipid concentration, then a drop from each liposome suspension was placed onto a Carbon Film Mesh Copper Grid (CF400-Cu, Electron Microscopy Science), and the excess suspension was removed with a filter paper. Staining was performed using aqueous uranyl acetate solution 1%.

**Cryoelectron Microscopy.** TEM grids of liposomes were prepared in a FEI Vitrobot using 3  $\mu\text{L}$  of sample adsorbed to freshly glow-discharged R2/2 Quantifoil grids. Grids were continuously blotted for 4–5 s in a 95% humidity chamber before plunge-freezing into liquid ethane. Data were then recorded on a Polara F30 FEG operating at 200 kV in a 4K Gatan Ultrascan CCD (charge-coupled device) in low-dose mode. CD images were recorded between 0.5 and 5.0  $\mu\text{m}$  defocus at a normal magnification of 39 000 $\times$  and at 3.5  $\text{\AA}/\text{pixel}$  (1  $\text{\AA}$  = 0.1 nm) and had a maximum electron dose of <25 electrons/ $\text{\AA}^2$ .

**SDS-PAGE Electrophoresis.** Proteins associated with 0.05  $\mu\text{M}$  of liposomes were mixed with Protein Solving Buffer (Fisher Scientific) for a final volume of 40  $\mu\text{L}$  and boiled for 5 min at 90 °C. Samples were then loaded in 4–20% Precise Tris-HEPES Protein Gel (Thermo Scientific). The gel was run for 1 h at 100 V, until the proteins neared the end of the gel, in 50 times diluted Tris-HEPES SDS Buffer (Thermo Scientific). Staining was performed with EZ Blue Gel Staining reagent (Sigma Life Science) overnight followed by washing in distilled water for 2 h.

**Quantification of Adsorbed Proteins.** Proteins associated with recovered liposomes were quantified by BCA Protein assay kit, as described earlier. Pb values, expressed as  $\mu\text{g}$  of protein/ $\mu\text{M}$  lipid were then calculated and represented as the average  $\pm$  standard error of three independent experiments. In the case of targeted liposomes the amount of protein contributed by the conjugated anti-MUC1 Ab (28.86  $\mu\text{g}$  Ab/ $\mu\text{mol}$  lipid).

**Mass Spectrometry.** Proteins associated with 0.05  $\mu\text{M}$  of liposomes were mixed with Protein Solving Buffer (Fisher Scientific) for a final volume of 25  $\mu\text{L}$  and boiled for 5 min at 90 °C.

Samples were then loaded in 10% Precise Tris-HEPES Protein Gel (Thermo Scientific). The gel was run for 3–5 min 100 V, in 50 times diluted Tris-HEPES SDS Buffer (Thermo Scientific). Staining was performed with EZ Blue Gel Staining reagent (Sigma Life Science) overnight followed by washing in distilled water for 2 h.

Bands of interest were excised from the gel and dehydrated using acetonitrile followed by vacuum centrifugation. Dried gel pieces were reduced with 10 mM dithiothreitol and alkylated with 55 mM iodoacetamide. Gel pieces were then washed alternately with 25 mM ammonium bicarbonate followed by acetonitrile. This was repeated, and the gel pieces dried by vacuum centrifugation. Samples were digested with trypsin overnight at 37 °C.

Digested samples were analyzed by LC–MS/MS using an UltiMate 3000 Rapid Separation LC (RSLC, Dionex Corporation, Sunnyvale, CA) coupled to a LTQ Velos Pro (Thermo Fisher Scientific, Waltham, MA) mass spectrometer. Peptide mixtures were separated using a gradient from 92% A (0.1% FA in water) and 8% B (0.1% FA in acetonitrile) to 33% B, in 44 min at 300 nL min<sup>-1</sup>, using a 250 mm × 75 μm i.d. 1.7 μm BEH C18, analytical column (Waters). Peptides were selected for fragmentation automatically by data dependent analysis. Data produced were searched using Mascot (Matrix Science UK), against the [Uniprot] database with taxonomy of [mouse] selected. Data were validated using Scaffold (Proteome Software, Portland, OR).

The Scaffold software (version 4.3.2, Proteome Software Inc.) was used to validate MS/MS based peptide and protein identifications and for relative quantification based on spectral counting. Peptide identifications were accepted if they could be established at greater than 95.0% probability by the Peptide Prophet algorithm with Scaffold delta-mass correction. Protein identifications were accepted if they could be established at greater than 99.0% probability and contained at least 2 identified peptides. Protein probabilities were assigned by the Protein Prophet algorithm. Proteins that contained similar peptides and could not be differentiated based on MS/MS analysis alone were grouped to satisfy the principles of parsimony. Semiquantitative assessment of the protein amounts was conducted using normalized spectral countings, NSCs, provided by Scaffold Software. The mean value of NSCs obtained in the three experimental replicates for each protein was normalized to the protein MW and expressed as a relative quantity by applying the following equation:<sup>19</sup>

$$MWNSC_k = \frac{(NSC/MW)_k}{\sum_{i=1}^N (NSC/MW)_i} \times 100 \quad (1)$$

where,  $MWNSC_k$  is the percentage molecular weight normalized NSC for protein k and MW is the molecular weight in kDa for protein k. This equation takes into consideration the protein size and evaluates the contribution of each protein reflecting its relative protein abundance (RPA).

**Internalization Studies.** C33a, a human, cervix carcinoma cell line (ATCC, USA) and MCF-7, human breast cancer cells (ATCC, USA) were used for the *in vitro* internalization studies. C33a cells were cultured in advanced RPMI-1640 (Roswell Park Memorial Institute) supplemented with 10% FBS (Fetal Bovine Serum), 1% L-Glutamine and 1% penicillin/streptomycin. MCF-7 cells were grown in MEM (Minimum Essential Media) supplemented with 10% FBS and 1% penicillin/streptomycin. Cells were grown in a humidified 37 °C/5% CO<sub>2</sub> incubator and passaged when they reached 80% confluence for a maximum of 20 passages, in order to maintain exponential growth.

MCF7 cells or C33a cells were seeded onto a coated glass bottom, 8 well chamber slide (Millicell EZ SLIDE, Merck-Millipore) (8000 cells/well). After 24 h of cell culture expansion, cells were transfected in serum free conditions with 0.15 mM of either DiD-labeled bare liposomes, liposomes recovered from intravenous injection into CD-1 mice or from *in vitro* incubation with isolated plasma for 1 h and 24 h. Naïve cells were used as controls. For the 24 h experiment, FBS was added 4 h after incubation to each well to achieve a final serum concentration

of 10% and cells were incubated at 37% in 5% CO<sub>2</sub> for 20 h. The cells were then washed three times with PBS. After that, cells were fixed by methanol precooled in –20 °C. Slides were mounted with Vectashield medium containing DAPI (Vector Laboratories) to stain the nuclei and coverslips were added. Images were collected on a Leica TCS SP5 AOBs inverted confocal using a 63× oil objective. The confocal settings were as follows, pinhole 1 airy unit, scan speed 1000 Hz unidirectional, format 1024 × 1024. Images were collected using the 405 nm (20%) and 633 nm (20%) laser lines, respectively. To eliminate cross-talk between channels, the images were collected sequentially. ImageJ (Fiji distribution) software was used to determine the fluorescence intensity.

To further confirm that the internalization of targeted liposomes was due to the interaction of Ab with MUC-1 antigen, MCF7 cells and C33a cells were also incubated at 37% in 5% CO<sub>2</sub> for 1 h with DiD-labeled targeted liposomes (before their interaction with plasma proteins) (Figure S6). Cells were then washed three times with PBS and fixed by methanol precooled in –20 °C. Slides were mounted with Vectashield medium containing DAPI (Vector Laboratories) to stain the nuclei and coverslips were added. Images were collected on a Leica TCS SP5 AOBs inverted confocal microscope as described for the 24 h internalization experiment.

**Statistical Analysis.** Statistical analysis of the data was performed using IBM SPSS Statistics software. One-way analysis of variance (ANOVA) followed by the Tukey multiple comparison test were used and *p* values <0.05 were considered significant.

**Conflict of Interest:** The authors declare no competing financial interest.

**Acknowledgment.** This research was partially funded by the Marie Skłodovkaya-Curie Initial Training Network *PathChooser* (PITN-GA-2013-608373). The University of Manchester Bioimaging Facility microscopes used in this study were purchased with grants from the BBSRC, Wellcome Trust and the University of Manchester Strategic Fund. Authors wish to acknowledge Dr. P. March from the Bioimaging Facility. The authors also wish to thank the staff in the Faculty of Life Sciences EM Facility for their assistance and the Wellcome Trust for equipment grant support to the EM Facility. In addition, Mass Spectrometry Facility staff at the University of Manchester for their assistance and Mr. M. Sylianides for his help with the liposome illustrations.

**Supporting Information Available:** Figure S1: Preparation of Ab-targeted liposomes by the postinsertion method; Figure S2: Comparison of the commercial mouse plasma used for the *in vitro* studies with the mouse plasma obtained from CD-1 mice; Figure S3: Separation of protein corona-coated liposomes from unbound and weakly bound proteins; Figure S4: Relative protein abundance (RPA) of fibrinogen alpha, beta and gamma chains in the *in vitro* and *in vivo* protein coronas formed on liposomes; Figure S5: Structural characterization of protein corona formation *in vitro* and *in vivo* by electron microscopy; Figure S6: Cellular uptake studies of DiD labeled liposomes and protein-coated liposomes recovered from the circulation of CD-1 mice 10 min postinjection and from *in vitro* incubation with isolated plasma; Table S1: Comparison of liposome physicochemical characteristics before and after their interaction with CD-1 mouse plasma *in vitro* and *in vivo*. The Supporting Information is available free of charge on the ACS Publications website at DOI: 10.1021/acsnano.5b03300.

## REFERENCES AND NOTES

- Cedervall, T.; Lynch, I.; Lindman, S.; Berggard, T.; Thulin, E.; Nilsson, H.; Dawson, K. A.; Linse, S. Understanding the Nanoparticle-Protein Corona Using Methods to Quantify Exchange Rates and Affinities of Proteins for Nanoparticles. *Proc. Natl. Acad. Sci. U. S. A.* **2007**, *104*, 2050–2055.
- Ashby, J.; Schachermeyer, S.; Pan, S. Q.; Zhong, W. W. Dissociation-Based Screening of Nanoparticle-Protein Interaction Via Flow Field-Flow Fractionation. *Anal. Chem.* **2013**, *85*, 7494–7501.

3. Hu, W.; Peng, C.; Lv, M.; Li, X.; Zhang, Y.; Chen, N.; Fan, C.; Huang, Q. Protein Corona-Mediated Mitigation of Cytotoxicity of Graphene Oxide. *ACS Nano* **2011**, *5*, 3693–3700.
4. Dobrovolskaia, M. A.; Patri, A. K.; Zheng, J.; Clogston, J. D.; Ayub, N.; Aggarwal, P.; Neun, B. W.; Hall, J. B.; McNeil, S. E. Interaction of Colloidal Gold Nanoparticles with Human Blood: Effects on Particle Size and Analysis of Plasma Protein Binding Profiles. *Nanomedicine* **2009**, *5*, 106–117.
5. Ge, C. C.; Du, J. F.; Zhao, L. N.; Wang, L. M.; Liu, Y.; Li, D. H.; Yang, Y. L.; Zhou, R. H.; Zhao, Y. L.; Chai, *et al.* Binding of Blood Proteins to Carbon Nanotubes Reduces Cytotoxicity. *Proc. Natl. Acad. Sci. U. S. A.* **2011**, *108*, 16968–16973.
6. Wang, F.; Yu, L.; Monopoli, M. P.; Sandin, P.; Mahon, E.; Salvati, A.; Dawson, K. A. The Biomolecular Corona Is Retained During Nanoparticle Uptake and Protects the Cells from the Damage Induced by Cationic Nanoparticles until Degraded in the Lysosomes. *Nanomedicine* **2013**, *9*, 1159–1168.
7. Lesniak, A.; Fenaroli, F.; Monopoli, M. R.; Aberg, C.; Dawson, K. A.; Salvati, A. Effects of the Presence or Absence of a Protein Corona on Silica Nanoparticle Uptake and Impact on Cells. *ACS Nano* **2012**, *6*, 5845–5857.
8. Jiang, X.; Weise, S.; Hafner, M.; Rocker, C.; Zhang, F.; Parak, W. J.; Nienhaus, G. U. Quantitative Analysis of the Protein Corona on FePt Nanoparticles Formed by Transferrin Binding. *J. R. Soc., Interface* **2010**, *7*, S5–S13.
9. Gessner, A.; Lieske, A.; Paulke, B. R.; Müller, R. H. Functional Groups on Polystyrene Model Nanoparticles: Influence on Protein Adsorption. *J. Biomed. Mater. Res.* **2003**, *65A*, 319–326.
10. Caracciolo, G.; Callipo, L.; De Sanctis, S. C.; Cavaliere, C.; Pozzi, D.; Lagana, A. Surface Adsorption of Protein Corona Controls the Cell Internalization Mechanism of Dc-Chol-Dope/DNA Lipoplexes in Serum. *Biochim. Biophys. Acta, Biomembr.* **2010**, *1798*, 536–543.
11. Tenzer, S.; Docter, D.; Kuharev, J.; Musyanovych, A.; Fetz, V.; Hecht, R.; Schlenk, F.; Fischer, D.; Kiouptsi, K.; Reinhardt, C.; *et al.* Rapid Formation of Plasma Protein Corona Critically Affects Nanoparticle Pathophysiology. *Nat. Nanotechnol.* **2013**, *8*, 772–781.
12. Salvati, A.; Pitek, A. S.; Monopoli, M. P.; Prapainop, K.; Bombelli, F. B.; Hristov, D. R.; Kelly, P. M.; Aberg, C.; Mahon, E.; Dawson, K. A. Transferrin-Functionalized Nanoparticles Lose Their Targeting Capabilities When a Biomolecule Corona Adsorbs on the Surface. *Nat. Nanotechnol.* **2013**, *8*, 137–143.
13. Mirshafiee, V.; Mahmoudi, M.; Lou, K.; Cheng, J.; Kraft, M. L. Protein Corona Significantly Reduces Active Targeting Yield. *Chem. Commun.* **2013**, *49*, 2557–2559.
14. Dai, Q.; Walkey, C.; Chan, W. C. Polyethylene Glycol Backfilling Mitigates the Negative Impact of the Protein Corona on Nanoparticle Cell Targeting. *Angew. Chem., Int. Ed.* **2014**, *53*, 5093–5096.
15. Al-Ahmady, Z. S.; Chaloin, O.; Kostarelos, K. Monoclonal Antibody-Targeted, Temperature-Sensitive Liposomes: *In Vivo* Tumor Chemotherapeutics in Combination with Mild Hyperthermia. *J. Controlled Release* **2014**, *196*, 332–343.
16. Allen, T. M.; Hansen, C. Pharmacokinetics of Stealth Versus Conventional Liposomes: Effect of Dose. *Biochim. Biophys. Acta, Biomembr.* **1991**, *1068*, 133–141.
17. Allen, T. M.; Hansen, C.; Martin, F.; Redemann, C.; Yau-Young, A. Liposomes Containing Synthetic Lipid Derivatives of Poly(Ethylene Glycol) Show Prolonged Circulation Half-Lives *In Vivo*. *Biochim. Biophys. Acta, Biomembr.* **1991**, *1066*, 29–36.
18. Papahadjopoulos, D.; Allen, T. M.; Gabizon, A.; Mayhew, E.; Matthay, K.; Huang, S. K.; Lee, K. D.; Woodle, M. C.; Lasic, D. D.; Redemann, C.; *et al.* Sterically Stabilized Liposomes: Improvements in Pharmacokinetics and Antitumor Therapeutic Efficacy. *Proc. Natl. Acad. Sci. U. S. A.* **1991**, *88*, 11460–11464.
19. Pozzi, D.; Colapicchioni, V.; Caracciolo, G.; Piovesana, S.; Capriotti, A. L.; Palchetti, S.; De Grossi, S.; Riccioli, A.; Amenitsch, H.; Lagana, A. Effect of Polyethyleneglycol (Peg) Chain Length on the Bio-Nano-Interactions between Pegylated Lipid Nanoparticles and Biological Fluids: From Nanostructure to Uptake in Cancer Cells. *Nanoscale* **2014**, *6*, 2782–2792.
20. Dobrovolskaia, M. A.; Neun, B. W.; Man, S.; Ye, X.; Hansen, M.; Patri, A. K.; Crist, R. M.; McNeil, S. E. Protein Corona Composition Does Not Accurately Predict Hematocompatibility of Colloidal Gold Nanoparticles. *Nanomedicine* **2014**, *10*, 1453–1463.
21. Gref, R.; Luck, M.; Quellec, P.; Marchand, M.; Dellacherie, E.; Harnisch, S.; Blunk, T.; Müller, R. H. 'Stealth' Corona-Core Nanoparticles Surface Modified by Polyethylene Glycol (Peg): Influences of the Corona (Peg Chain Length and Surface Density) and of the Core Composition on Phagocytic Uptake and Plasma Protein Adsorption. *Colloids Surf., B* **2000**, *18*, 301–313.
22. Mishra, S.; Webster, P.; Davis, M. E. Pegylation Significantly Affects Cellular Uptake and Intracellular Trafficking of Non-Viral Gene Delivery Particles. *Eur. J. Cell Biol.* **2004**, *83*, 97–111.
23. Perche, F.; Torchilin, V. P. Recent Trends in Multifunctional Liposomal Nanocarriers for Enhanced Tumor Targeting. *J. Drug Delivery* **2013**, *2013*, 705265.
24. Semple, S. C.; Chonn, A.; Cullis, P. R. Influence of Cholesterol on the Association of Plasma Proteins with Liposomes. *Biochemistry* **1996**, *35*, 2521–2525.
25. Chonn, A.; Semple, S. C.; Cullis, P. R. Association of Blood Proteins with Large Unilamellar Liposomes *In Vivo*. Relation to Circulation Lifetimes. *J. Biol. Chem.* **1992**, *267*, 18759–18765.
26. Chonn, A.; Semple, S. C.; Cullis, P. R. Separation of Large Unilamellar Liposomes from Blood Components by a Spin Column Procedure: Towards Identifying Plasma Proteins Which Mediate Liposome Clearance *In Vivo*. *Biochim. Biophys. Acta, Biomembr.* **1991**, *1070*, 215–222.
27. Diederichs, J. E. Plasma Protein Adsorption Patterns on Liposomes: Establishment of Analytical Procedure. *Electrophoresis* **1996**, *17*, 607–611.
28. Mahmoudi, M.; Lynch, I.; Eftejadi, M. R.; Monopoli, M. P.; Bombelli, F. B.; Laurent, S. Protein-Nanoparticle Interactions: Opportunities and Challenges. *Chem. Rev.* **2011**, *111*, 5610–5637.
29. Sakulkhu, U.; Maurizi, L.; Mahmoudi, M.; Motazacker, M.; Vries, M.; Gramoun, A.; Ollivier Beuzelin, M. G.; Vallee, J. P.; Rezaee, F.; Hofmann, H. *Ex Situ* Evaluation of the Composition of Protein Corona of Intravenously Injected Superparamagnetic Nanoparticles in Rats. *Nanoscale* **2014**, *6*, 11439–11450.
30. Barenholz, Y. Doxil(R)–the First Fda-Approved Nano-Drug: Lessons Learned. *J. Controlled Release* **2012**, *160*, 117–134.
31. Soloman, R.; Gabizon, A. A. Clinical Pharmacology of Liposomal Anthracyclines: Focus on Pegylated Liposomal Doxorubicin. *Clin. Lymphoma Myeloma* **2008**, *8*, 21–32.
32. Lozano, N.; Al-Ahmady, Z. S.; Beziere, N. S.; Ntziachristos, V.; Kostarelos, K. Monoclonal Antibody-Targeted Pegylated Liposome-Icg Encapsulating Doxorubicin as a Potential Theranostic Agent. *Int. J. Pharm.* **2015**, *482*, 2–10.
33. Barran-Berdon, A. L.; Pozzi, D.; Caracciolo, G.; Capriotti, A. L.; Caruso, G.; Cavaliere, C.; Riccioli, A.; Palchetti, S.; Lagana, A. Time Evolution of Nanoparticle-Protein Corona in Human Plasma: Relevance for Targeted Drug Delivery. *Langmuir* **2013**, *29*, 6485–6494.
34. Docter, D.; Distler, U.; Storck, W.; Kuharev, J.; Wunsch, D.; Hahlbrock, A.; Knauer, S. K.; Tenzer, S.; Stauber, R. H. Quantitative Profiling of the Protein Coronas That Form around Nanoparticles. *Nat. Protoc.* **2014**, *9*, 2030–2044.
35. Lundqvist, M.; Stigler, J.; Cedervall, T.; Berggard, T.; Flanagan, M. B.; Lynch, I.; Elia, G.; Dawson, K. The Evolution of the Protein Corona around Nanoparticles: A Test Study. *ACS Nano* **2011**, *5*, 7503–7509.
36. Pitek, A. S.; O'Connell, D.; Mahon, E.; Monopoli, M. P.; Bombelli, F. B.; Dawson, K. A. Transferrin Coated Nanoparticles: Study of the Bionano Interface in Human Plasma. *PLoS One* **2012**, *7*, e40685.

37. Johnstone, S. A.; Masin, D.; Mayer, L.; Bally, M. B. Surface-Associated Serum Proteins Inhibit the Uptake of Phosphatidylserine and Poly(Ethylene Glycol) Liposomes by Mouse Macrophages. *Biochim. Biophys. Acta, Biomembr.* **2001**, *1513*, 25–37.
38. Wolfram, J.; Suri, K.; Yang, Y.; Shen, J.; Celia, C.; Fresta, M.; Zhao, Y.; Shen, H.; Ferrari, M. Shrinkage of Pegylated and Non-Pegylated Liposomes in Serum. *Colloids Surf., B* **2013**, *114C*, 294–300.
39. Loomis, K.; Smith, B.; Feng, Y.; Garg, H.; Yavlovich, A.; Campbell-Massa, R.; Dimitrov, D. S.; Blumenthal, R.; Xiao, X.; Puri, A. Specific Targeting to B Cells by Lipid-Based Nanoparticles Conjugated with a Novel Cd22-Scfv. *Exp. Mol. Pathol.* **2010**, *88*, 238–249.
40. Deng, Z. J.; Liang, M.; Monteiro, M.; Toth, I.; Minchin, R. F. Nanoparticle-Induced Unfolding of Fibrinogen Promotes Mac-1 Receptor Activation and Inflammation. *Nat. Nanotechnol.* **2011**, *6*, 39–44.
41. Min, Y.; Akbulut, M.; Kristiansen, K.; Golan, Y.; Israelachvili, J. The Role of Interparticle and External Forces in Nanoparticle Assembly. *Nat. Mater.* **2008**, *7*, 527–538.
42. Walkey, C. D.; Olsen, J. B.; Song, F.; Liu, R.; Guo, H.; Olsen, D. W.; Cohen, Y.; Emili, A.; Chan, W. C. Protein Corona Fingerprinting Predicts the Cellular Interaction of Gold and Silver Nanoparticles. *ACS Nano* **2014**, *8*, 2439–2455.
43. Rocker, C.; Potzl, M.; Zhang, F.; Parak, W. J.; Nienhaus, G. U. A Quantitative Fluorescence Study of Protein Monolayer Formation on Colloidal Nanoparticles. *Nat. Nanotechnol.* **2009**, *4*, 577–580.
44. Xia, X. R.; Monteiro-Riviere, N. A.; Mathur, S.; Song, X.; Xiao, L.; Oldenberg, S. J.; Fadeel, B.; Riviere, J. E. Mapping the Surface Adsorption Forces of Nanomaterials in Biological Systems. *ACS Nano* **2011**, *5*, 9074–9081.
45. Kapralov, A. A.; Feng, W. H.; Amoscato, A. A.; Yanamala, N.; Balasubramanian, K.; Winnica, D. E.; Kisin, E. R.; Kotchey, G. P.; Gou, P.; Sparvero, L. J.; Ray, P.; *et al.* Adsorption of Surfactant Lipids by Single-Walled Carbon Nanotubes in Mouse Lung Upon Pharyngeal Aspiration. *ACS Nano* **2012**, *6*, 4147–4156.
46. Linse, S.; Cabaleiro-Lago, C.; Xue, W. F.; Lynch, I.; Lindman, S.; Thulin, E.; Radford, S. E.; Dawson, K. A. Nucleation of Protein Fibrillation by Nanoparticles. *Proc. Natl. Acad. Sci. U. S. A.* **2007**, *104*, 8691–8696.
47. Hsieh, S. C.; Chang, C. W.; Chou, H. H. Gold Nanoparticles as Amyloid-Like Fibrillogenesis Inhibitors. *Colloids Surf., B* **2013**, *112*, 525–529.
48. Mahmoudi, M.; Quinlan-Pluck, F.; Monopoli, M. P.; Sheibani, S.; Vali, H.; Dawson, K. A.; Lynch, I. Influence of the Physicochemical Properties of Superparamagnetic Iron Oxide Nanoparticles on Amyloid Beta Protein Fibrillation in Solution. *ACS Chem. Neurosci.* **2013**, *4*, 475–485.
49. Sen, S.; Konar, S.; Pathak, A.; Dasgupta, S.; DasGupta, S. Effect of Functionalized Magnetic MnFe<sub>2</sub>O<sub>4</sub> Nanoparticles on Fibrillation of Human Serum Albumin. *J. Phys. Chem. B* **2014**, *118*, 11667–11676.
50. Caracciolo, G.; Pozzi, D.; Capriotti, A. L.; Cavaliere, C.; Piovesana, S.; La Barbera, G.; Amici, A.; Lagana, A. The Liposome-Protein Corona in Mice and Humans and Its Implications for *in Vivo* Delivery. *J. Mater. Chem. B* **2014**, *2*, 7419–7428.
51. Simberg, D.; Park, J. H.; Karmali, P. P.; Zhang, W. M.; Merkulov, S.; McCrae, K.; Bhatia, S. N.; Sailor, M.; Ruoslahti, E. Differential Proteomics Analysis of the Surface Heterogeneity of Dextran Iron Oxide Nanoparticles and the Implications for Their *in Vivo* Clearance. *Biomaterials* **2009**, *30*, 3926–3933.
52. Caracciolo, G.; Cardarelli, F.; Pozzi, D.; Salomone, F.; Maccari, G.; Bardi, G.; Capriotti, A. L.; Cavaliere, C.; Papi, M.; Lagana, A. Selective Targeting Capability Acquired with a Protein Corona Adsorbed on the Surface of 1,2-Dioleoyl-3-Trimethylammonium Propane/DNA Nanoparticles. *ACS Appl. Mater. Interfaces* **2013**, *5*, 13171–13179.
53. Pozzi, D.; Caracciolo, G.; Capriotti, A. L.; Cavaliere, C.; Piovesana, S.; Colapicchioni, V.; Palchetti, S.; Riccioli, A.; Lagana, A. A Proteomics-Based Methodology to Investigate the Protein Corona Effect for Targeted Drug Delivery. *Mol. Biosyst.* **2014**, *11*, 2815–2819.
54. Caracciolo, G. Liposome-Protein Corona in a Physiological Environment: Challenges and Opportunities for Targeted Delivery of Nanomedicines. *Nanomedicine* **2015**, *11*, 543–557.
55. Zarschler, K.; Prapainop, K.; Mahon, E.; Rocks, L.; Bramini, M.; Kelly, P. M.; Stephan, H.; Dawson, K. A. Diagnostic Nanoparticle Targeting of the EGF-Receptor in Complex Biological Conditions Using Single-Domain Antibodies. *Nanoscale* **2014**, *6*, 6046–6056.
56. Dai, Q.; Yan, Y.; Ang, C. S.; Kempe, K.; Kamphuis, M. M.; Dodds, S. J.; Caruso, F. Monoclonal Antibody-Functionalized Multilayered Particles: Targeting Cancer Cells in the Presence of Protein Coronas. *ACS Nano* **2015**, *9*, 2876–2885.
57. Hood, J. D.; Bednarski, M.; Frausto, R.; Guccione, S.; Reisfeld, R. A.; Xiang, R.; Cheres, D. A. Tumor Regression by Targeted Gene Delivery to the Neovasculature. *Science* **2002**, *296*, 2404–2407.
58. Drummond, D. C.; Noble, C. O.; Guo, Z.; Hayes, M. E.; Connolly-Ingram, C.; Gabriel, B. S.; Hann, B.; Liu, B.; Park, J. W.; Hong, K.; *et al.* Development of a Highly Stable and Targetable Nanoliposomal Formulation of Topotecan. *J. Controlled Release* **2010**, *141*, 13–21.
59. Cheng, W. W.; Allen, T. M. Targeted Delivery of Anti-Cd19 Liposomal Doxorubicin in B-Cell Lymphoma: A Comparison of Whole Monoclonal Antibody, Fab' Fragments and Single Chain Fv. *J. Controlled Release* **2008**, *126*, 50–58.
60. Gabizon, A.; Horowitz, A. T.; Goren, D.; Tzemach, D.; Shmeeda, H.; Zalipsky, S. *In Vivo* Fate of Folate-Targeted Polyethylene-Glycol Liposomes in Tumor-Bearing Mice. *Clin. Cancer Res.* **2003**, *9*, 6551–6559.
61. Al-Ahmady, Z. S.; Al-Jamal, W. T.; Bossche, J. V.; Bui, T. T.; Drake, A. F.; Mason, A. J.; Kostarellos, K. Lipid-Peptide Vesicle Nanoscale Hybrids for Triggered Drug Release by Mild Hyperthermia *in Vitro* and *in Vivo*. *ACS Nano* **2012**, *6*, 9335–9346.
62. Needham, D.; Anyarambhatla, G.; Kong, G.; Dewhirst, M. W. A New Temperature-Sensitive Liposome for Use with Mild Hyperthermia: Characterization and Testing in a Human Tumor Xenograft Model. *Cancer Res.* **2000**, *60*, 1197–1201.
63. Kong, G.; Anyarambhatla, G.; Petros, W. P.; Braun, R. D.; Colvin, O. M.; Needham, D.; Dewhirst, M. W. Efficacy of Liposomes and Hyperthermia in a Human Tumor Xenograft Model: Importance of Triggered Drug Release. *Cancer Res.* **2000**, *60*, 6950–6957.